

# Action-OOD: An End-to-End Skeleton-Based Model for Robust Out-of-Distribution Human Action Detection

Jing Xu<sup>a,b</sup>, Anqi Zhu<sup>c</sup>, Jingyu Lin<sup>a,b</sup>, Qihong Ke<sup>b</sup>, Cunjian Chen<sup>a,b,\*</sup>

<sup>a</sup>Monash Suzhou Research Institute, Suzhou, 215000, Jiangsu, China

<sup>b</sup>Department of Data Science and AI, Monash University, Victoria, 3800, Melbourne, Australia

<sup>c</sup>Department of Computing and Information Systems, University of Melbourne, Parkville VIC, 3052, Melbourne, Australia

---

## Abstract

Human action recognition is a crucial task in computer vision systems. However, in real-world scenarios, human actions often fall outside the distribution of training data, requiring a model to both recognize in-distribution (ID) actions and reject out-of-distribution (OOD) ones. Despite its importance, there has been limited research on OOD detection in human actions. Existing works on OOD detection mainly focus on image data with RGB structure, and many methods are post-hoc in nature. While these methods are convenient and computationally efficient, they often lack sufficient accuracy and fail to consider the presence of OOD samples. To address these challenges, we propose a novel end-to-end skeleton-based model called Action-OOD, specifically designed for OOD human action detection. Unlike some existing approaches that may require prior knowledge of existing OOD data distribution, our model solely utilizes in-distribution (ID) data during the training stage, effectively mitigating the overconfidence issue prevalent in OOD detection. We introduce an attention-based feature fusion block, which enhances the model's capability to recognize unknown classes while preserving classification accuracy for known classes. Further, we present a novel energy-based loss function and successfully integrate it with the traditional cross-entropy loss to maximize the separation of data distributions between ID and OOD. Through extensive experiments conducted on NTU-RGB+D 60, NTU-RGB+D 120, and Kinetics-400 datasets, we demonstrate the superior performance of our proposed approach compared to state-of-the-art methods. Our findings underscore the effectiveness of classic OOD detection techniques in the context of skeleton-based action recognition tasks, offering promising avenues for future research in this field. Code will be available at: <https://github.com/YilliaJing/Action-OOD.git>.

*Keywords:* Action Recognition, Out-of-Distribution Detection, Graph Neural Networks, Energy-based Theory

---

## 1. Introduction

Human-centric visual understanding enhances the development of intelligent machines, enabling humans to accomplish greater tasks and improve their quality of life. Deep learning-based models have shown remarkable performance in supervised human action classification tasks. In skeleton-based human action datasets, this task can

be solved as a typical spatio-temporal modeling problem (Yan et al., 2018; Chen et al., 2021; Cheng et al., 2020). Although these methods have achieved high accuracy in supervised classification problems, they still lack consideration for out-of-distribution (OOD) issues. An important assumption in these approaches is that the distribution of the training set is similar to that of the test set. However, this can not always be achieved in practice. When these models are applied to recognize samples outside the distribution of the training set, they may exhibit overconfidence by selecting a category from the known distribu-

---

\*Corresponding author: Tel.: +1-517-303-2723;  
e-mail: [cunjian.chen@monash.edu](mailto:cunjian.chen@monash.edu)

tion (Yu et al., 2024). Hence, it is essential for such models to be aware of the boundaries of learning for safety concerns (Nalisnick et al., 2019), ensuring the robustness of computer vision systems. How to deal with this OOD detection problem has attracted widespread attention in fields such as autonomous driving (Geiger et al., 2012) and medical image analysis (Schlegl et al., 2017).

Works in OOD detection focus on OOD samples caused by semantic shift, aiming to determine whether a sample belongs to a category included in the training dataset. This task presents two challenges: quantifying the differences between in-distribution (ID) and OOD samples, and distinguishing them based on their expressions. For the first challenge, one typical approach is score measuring methods (Hendrycks and Gimpel, 2017), such as the softmax confidence score (Hendrycks and Gimpel, 2017). Inputs with low softmax confidence scores are classified as OOD. However, neural networks can produce arbitrarily high softmax confidence scores for inputs far from the training data (Nguyen et al., 2015). To address this, the energy score is proposed for OOD detection. It can be derived from a purely discriminative classification model without explicitly relying on a density estimator. Experiments show that it outperforms softmax-based score measuring methods.

Based on such score measuring methods, a crucial issue is how to maximize the difference in score distributions between OOD and ID samples. To achieve this, difference amplification methods (Sun et al., 2021; Zhu et al., 2022) have been designed. However, these methods are mostly implemented in a post-hoc manner, meaning the model itself cannot inherently distinguish OOD samples. This does not fundamentally solve the problem of 'letting the model know what it knows.' Furthermore, these methods were originally designed for OOD detection in RGB-structured datasets. Their effectiveness in handling action recognition problems with skeleton structure data has not yet been investigated.

Furthermore, methods by Wu and et al. (2023) have attempted to achieve this goal by introducing OOD distribution information into the training stage. However, in practice, we cannot measure the specific categories of OOD. Similarly, when the OOD category itself expands, the overconfidence problem still remains. In summary, while these methods significantly improve the accuracy of OOD recognition, achieving this goal using an end-to-

end framework without prior OOD information remains challenging.

To address the limits and challenges mentioned above, we propose an end-to-end model called Action-OOD to deal with the out-of-distribution detection problem for skeleton-based action recognition. Considering that the state-of-the-art feature extractors for supervised skeleton-based recognition are well-developed, we focus on exploiting the extracted features to extend their adaptability for OOD detection while maintaining robust prediction performance for the supervised classes. We use HD-GCN (Lee et al., 2023), a prevailing backbone at present, as our main feature extractor. Based on its basic output, we first creatively applied a feature activation module that utilizes ASH (Djurisic and et al., 2023) to project the original features for fitting OOD detection in the training stage. Specifically, it filters useless information and amplifies the key feature dimensions to generate a more sensitive and accurate representation of abnormal detections. Then, regarding this as an orthogonal aggregation to the original features, we innovatively designed a feature fusion module, which integrates the original backbone outputs and the OOD-targeted activated features to enable the model to preserve a strong recognition ability for ID data while also nicely discriminating the potential OOD existences. To support the framework with end-to-end training, we suggested a meticulously designed learning loss that combines the energy function and cross-entropy information. This approach aims to improve the model's understanding of the energy score distribution in ID data, thereby further benefiting the accurate detection of OOD samples.

Our main contributions are summarized as follows:

- We propose Action-OOD, an end-to-end skeleton-based OOD detection model that addresses overconfidence by solely training on ID data.
- The attention-based feature fusion block is designed to enhance OOD detection accuracy while preserving classification ability for ID classes.
- We design an energy-based loss function, which can improve score differentiation between ID and OOD samples, thus effectively maximizing their distribution separations.
- The proposed model Action-OOD outperforms baselines on NTU-RGB+D 60, NTU-RGB+D 120, and

Kinetics-400 datasets in the human action OOD detection task.

The rest of the paper is organized as follows: Section 2 explains basic knowledge of skeleton-based action recognition tasks with GCNs and the theory of why energy score is most widely used in OOD detection. Section 3 introduces our proposed method in detail, including proposed framework, feature fusion block and loss function design. Section 4 mainly discusses the result of experiments. We offer conclusion and discuss future works in Section 5.

## 2. Related works

### 2.1. GCNs for Skeleton based Action Recognition

Human action recognition task is a typical problem in computer vision, which has wide applications in the real world including human-computer interaction (Nikam and Ambekar, 2016) and video surveillance (Jiang et al., 2015). Skeleton-based method has its unique advantages. The skeleton structure can provide more accurate node-level information and ignore the influence of background noise information, thus improving the prediction accuracy of recognition.

In the early phases of skeleton-based action recognition using deep learning methods, convolution neural networks (CNNs) (Chéron et al., 2015; Liu et al., 2017b; Simonyan and Zisserman, 2014), and recurrent neural networks (RNNs) (Wang and Wang, 2017; Liu et al., 2017a) were commonly utilized. However, these approaches had limitations as they didn’t fully leverage the structural arrangement of the joints.

After that, researchers build spatio-temporal architectures to handle this problem. Many works use handcrafted physically connected (PC) edges among human skeletons to extract spatial features (Chen et al., 2021; Cheng et al., 2020) and GCNs can handle this type of graph-structured data very well. The graph defined on the human skeleton is denoted as  $G(V, E)$ , with  $V$  representing the joint group and  $E$  representing the edge group. The representation of 3D time-series skeletal data is denoted as  $X \in \mathbb{R}^{C \times T \times |V|}$ , where  $|V|$  represents the number of joint nodes,  $C$  is the number of channel, and  $T$  denotes the temporal window size. The operation of GCN with an input feature map  $X$  can be described as follows:

$$\mathbf{F}_{\text{out}} = \mathbf{A}\mathbf{X}\Theta. \quad (1)$$

Here,  $\Theta$  denotes the pointwise convolution operation.  $A$  represents adjacency matrix that is initialized as  $\Lambda^{-\frac{1}{2}}\mathbf{A}\Lambda^{-\frac{1}{2}} \in \mathbb{R}^{N_g \times |V| \times |V|}$ , where  $\Lambda$  is a diagonal matrix for normalization and  $N_g = 3$  in experiments.

However, relying solely on PC edges for spatial relationships is insufficient, as it limits the receptive fields due to their heuristic and fixed nature. Additionally, the varying contributions of each edge must be considered, as the importance of joints in different body parts varies for specific actions. To address these issues, Hierarchically Decomposed Graph Convolutional Networks (HD-GCN) (Lee et al., 2023) were proposed. The graph convolution operation of HD-GCN is defined as:

$$\mathbf{F}_{\text{out}} = \sum_{g \in G} \mathbf{A}_g \mathbf{X} \Theta_g, \quad (2)$$

where  $G = \{g_{pc}, g_{sl}, g_{fc}\}$  denotes three graph subsets, and  $g_{pc}$ ,  $g_{sl}$ , and  $g_{fc}$  indicate physical connections, self-loops, and fully connected joint subsets, respectively. It represents three typical useful graph relationships to help explore spatial relationships between joints. The construction of these three kinds will be introduced in detail in section 3.1. With this operation, HD-GCN achieved an average Top-1 accuracy of 93.9% across three experimental datasets.

### 2.2. Methods for out-of-distribution detection

Research on out-of-distribution detection can be mainly categorized into two ways. First, we can define a scoring function that maps each input point to a single scalar, such that in-distribution and out-of-distribution data will have different distributions. Thus, we can identify the out-of-distribution samples by calculating this score. There are many works about how to define this kind of score for pre-trained neural networks. Hendrycks and Gimpel (2017) proposed the maximum predicted softmax probability (MSP). After that, Wu and et al. (2023) proved that the log of the MSP was equivalent to a special case of the free energy score. This indicates that there are some cases in ID and OOD data with similar MSP values but different energy scores. As a result, energy score has become one of the most widely used score measuring method.

Secondly, we can distinguish ID and OOD by trying to modify the feature captured by a pre-trained neural networks in a post-hoc way, which is usually applied to feature activations. Numerous experiments have shown that different feature activation methods can help differentiate ID and OOD. Sun et al. (2021) proposed rectified activation (ReAct) after observing that OOD data can trigger unit activation patterns that were significantly different from ID data in the penultimate layer of the model. Performing truncation can help drastically improve the separation of ID and OOD data. Zhu et al. (2022) found that some operations similar to Batch Normalization might increase the difference in scores (e.g., MSP and energy score) between ID and OOD data. DICE (Sun and Li, 2022) was proposed to address the shortcomings of redundant information expressed in the high space of neural networks. It attempted to define weights (i.e., weight  $\times$  activation) to sort and filter the nodes in the penultimate layer of the neural network for denoising. This further reduces the variance value of the ID and OOD data score distributions, making it easier to separate the peaks of the two distributions. Similar to the previous works, Djuric and et al. (2023) removed the top-K elements (usually a large portion over 50%) and adjust the remaining (e.g. 10%) activation values by scaling them up or straightly assign them a constant number. It achieves state-of-art performance on several benchmarks of image classification.

However, most of the first two kinds of methods are considered post-hoc. While they can reduce calculation costs than training another new specific OOD detection model, research by Liu et al. (2023) showed that they were still less competitive than some works that utilized OOD information in the training stage, such as works by Hendrycks et al. (2022) and Song et al. (2022). Additionally, these methods were initially designed for OOD detection in RGB-structured datasets. Their effectiveness in addressing action recognition problems with skeleton structure data has not yet been explored. In this work, we prove the validity of these methods on skeleton-based datasets and then take steps to solve these problems.

### 2.3. Energy-based out-of-distribution detection

In deep neural networks, out-of-distribution detection distinguishes samples that deviate from the training distribution. In this work, we only focus on the standard OOD

detection that concerns semantic shifts, in which OOD data is defined as test samples from semantic categories that were not seen during training. Ideally, the neural network should be able to reject such samples as OOD while maintaining strong classification performance on ID test samples belonging to seen training categories (Zhang and et al., 2023). To achieve this goal, a common approach is to utilize the data density function, denoted as  $p^{\text{in}}(x)$ , and identify instances with low likelihood as OOD. Nevertheless, prior studies have demonstrated that density functions estimated by deep generative models are not consistently reliable for OOD detection (Nalisnick et al., 2019).

Energy-based out-of-distribution detection employs an energy score for detection, where the difference of energies between ID and OOD facilitates separation. The energy score addresses a crucial issue associated with softmax confidence, which can lead to excessively high values for OOD examples (Hein et al., 2019).

Let us define a discriminate neural network  $f(x) : \mathbb{R}^D \rightarrow \mathbb{R}^K$ , which maps the input  $x$  to  $K$  real-valued numbers known as logits. Its energy score function  $E(x, f)$  over  $\mathbb{R}^D$  with softmax activation can be defined as follows:

$$E(\mathbf{x}; f) = -T \cdot \log \sum_i^K e^{f_i(\mathbf{x})/T}, \quad (3)$$

where  $T$  is the temperature parameter. It can also be proved that a model trained with negative log-likelihood (NLL) loss will push down energy for in-distribution data points and pull up for other labels (LeCun et al., 2006). Since cross-entropy loss can be implemented as NLL loss after the logSoftmax function, it will also push down the energy score of ID data. In other words, the ID sample will have a larger negative energy score  $-E(x; f)$  than the OOD sample.

## 3. Method

Our main objective is to achieve accurate human action OOD detection through an end-to-end framework without any other subsequent fine-tuning or post-hoc operations. The whole framework of the proposed skeleton-based OOD human action detection model is shown in Fig. 1.

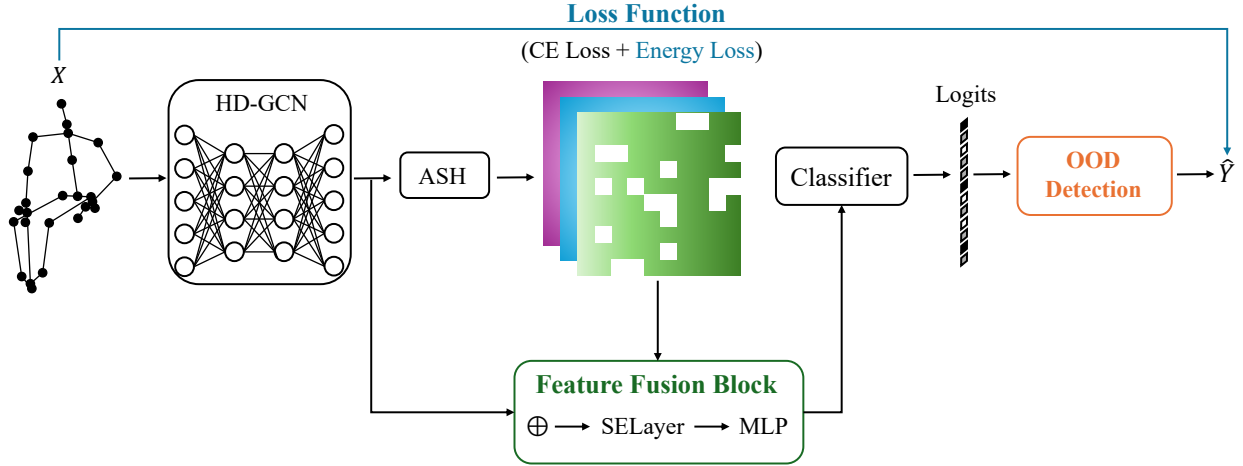


Figure 1: Framework of the proposed Action-OOD model. The symbol  $\oplus$  represents the vector concatenate operation.

It can be divided into three main steps of the end-to-end Action-OOD framework: Firstly, we use HD-GCN (Lee et al., 2023), a GCN framework that achieves state-of-the-art accuracy in ID classification, to perform feature extraction on skeleton data. Secondly, The extracted features are then activated and fused with the original ones. The function of the feature fusion block is to improve the recognition ability of OOD samples while preserving the original classification performance of ID data. Finally, it is fed into the classifier, and OOD detection is performed based on the classifier output logits as shown in Fig. 4. Besides, the whole model is trained by an energy-based loss function. Our work focuses on feature processing and OOD detection. Below, we will delve extensively into each of these components.

### 3.1. GCN-based feature extractor

Since many GCN based models have achieved great success in action recognition tasks, in this work we use existing models that perform best in ID data classification to extract embeddings from human skeleton data. It is an important step for a GCN based model to construct the graph topology in advance. A topology can bring great convenience to the spatial learning of the model while incorporating prior information thus improving the physical consistency of the model. Following the previous work by (Lee et al., 2023), we define three types of links for

joint connections, while keeping the number of nodes unchanged (see Fig. 2).

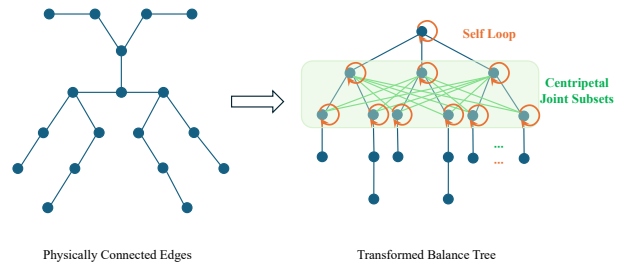


Figure 2: Description of the graph construction method. Taking the Kinetics dataset as an example, the left part is the visualized body joints and their physical connections. The right part is the transformed balance tree based on PC edges. The orange edges represent the self-loop of joints. Green edges represent fully connected edges within each centripetal joint subset.

Let us define  $G = \{g_{pc}, g_{sl}, g_{fc}\}$  as the three types of graph subsets. The first type of subset  $g_{pc}$  is physical connections, which are represented by blue lines between joints in Fig. 2. It represents the natural physical relationships in skeleton data. The second type  $g_{sl}$  is the self-loop, where nodes are connected to themselves. By incorporating self-loops, nodes are enabled to consider their own features during message passing in addition to relying on neighboring nodes' information, which helps stabilize the training process. Additionally, self-loops can be

regarded as a regularization mechanism to prevent overfitting, making them a commonly used method in graph neural network construction (Kipf and Welling, 2017).

The third type of subset is a hierarchical fully connected joints  $g_{fc}$ . We employ a balanced tree approach to re-represent the graph structure (as illustrated on the right side of Fig. 2). Fully connected edges are constructed between adjacent nodes across two levels of the balanced tree, based on the hierarchical level of the nodes. This approach considers that the characteristics of actions may correlate with features across various levels of the body’s hierarchical structure. Additionally, it expands the model’s receptive field spatially in the feature space, enhancing the model’s generalization ability. This approach has been widely proven to be effective in previous experiments. After that, for the input skeleton data  $X$ , the output feature maps  $F$  as:

$$F = f^{HD-GCN}(X, G). \quad (4)$$

### 3.2. Feature activation shaping and fusion

Following the previous work (Djurisic and et al., 2023), we utilize activation shaping (ASH) operation to filter out useless information in high-dimensional HD-GCN captured feature maps  $F$ , which can bring benefits to other downstream tasks (e.g. OOD detection). However, the difference is that we utilize it in the training stage to help the model itself distinguish OOD samples.

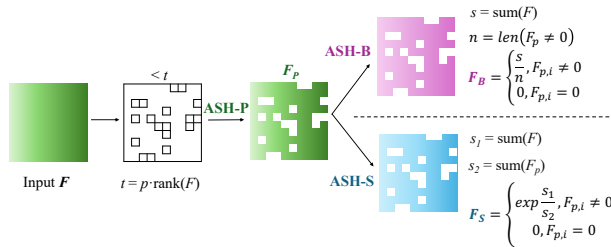


Figure 3: Process of Activation Shaping strategies. They prune the elements by pruning percentage and then conduct different strategies to assign values to the remaining elements.

There are three types of ASH strategies: ASH-P, ASH-B, and ASH-S. As shown in Fig. 3, for the input feature maps  $F$ , ASH-P only set values less than  $t$  into zero, ASH-B reset the non-zeros by binarization, and ASH-S set them with scaling. Details of these three strategies can be found

in supplementary material. The difference among them lies in the normalization strategies after pruning. In the experimental part, we show the results of all these three strategies in training. After that, we retain both the output feature maps and the pruning features:

$$\hat{F} = [F, \text{ASH}(F)], \quad (5)$$

where  $\text{ASH}(F)$  represents the results of any activation strategy acting on the feature maps  $F$ , and  $[\cdot, \cdot]$  denotes the process to concatenate two vectors into a single one. The concatenated features undergo two main operations in the feature fusion process: one SE layer (Hu et al., 2018) primarily aimed at enhancing the model’s sensitivity to channel features:

$$F^{SE} = \hat{F} \cdot \text{ReLU} \left( W_{fc} \cdot \underbrace{\frac{\sum_i^{k_h} \sum_j^{k_w} \hat{F}}{k_h \times k_w}}_{\text{average pool}} + b \right), \quad (6)$$

and the other MLP layer (Yu and et al., 2022):

$$F^{fuse} = \text{MLP}(F^{SE}). \quad (7)$$

Here,  $W_{fc}$  represents the learnable weights. At this stage, we have acquired the fused feature  $F^{fuse}$ . Experiments show that it can improve the recognition ability of unseen classes while ensuring the classification accuracy of seen classes.

### 3.3. OOD detection using logits

After the feature pruning and fusion process, the extracted features will be fed into a classifier:

$$\text{logits} = W'_{fc} \cdot \text{drop\_out}(F^{fuse}) + b'. \quad (8)$$

Here Eqn. 8 shows the classification operation after data fusion and  $W'_{fc}$  are the learnable weights. Then we get the logits ready for the downstream OOD detection task. The dimension of logits is equivalent to the total number of seen classes plus one unseen class. The detailed process of OOD detection is illustrated in Fig. 4.

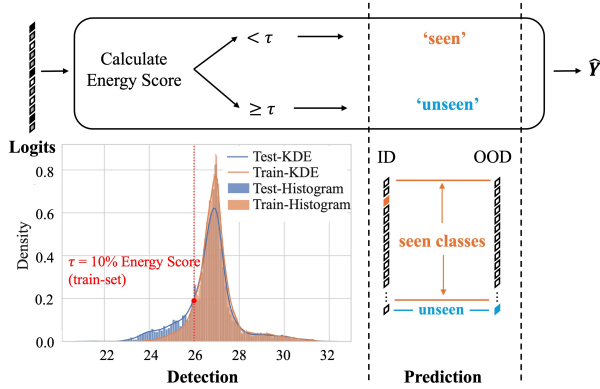


Figure 4: Explanation of OOD detection process. In the detection stage, the input is the logits from the previous feature extractor. Based on the Energy-based theory, the lower the score, the more likely the sample is the in-distribution.

For the input logits after the classifier, we measure the energy score of each sample using Eqn. 3: If the score is smaller than  $\tau$ , we will recognize it as ‘unseen’ for OOD and set the element value representing the probability that the sample belongs to the unknown category to 1. Otherwise, the probability of unseen will remain zero and others will be the value between 0 to 1. The value of parameter  $\tau$  is given based on the top 10% of energy scores on the training set. The assumption behind this is that the energy score of OOD after training is less than the energy score of 90% ID data. After that, we can get a vector  $\hat{Y}$  that represents the probability that the sample belongs to each class.

### 3.4. Energy based loss function

As stated in section 2.2, although the model trained with cross-entropy loss will lower the energy score value of OOD data, the gap between the two distributions may not always be optimal for detection. Therefore, we propose an energy-bounded learning objective and combine it with traditional cross-entropy loss:

$$L = - \sum_{logits_{in}} P(logits_{in}) \log f(logits_{in}) + \alpha \cdot \mathbb{E}_{(logits_{in}, y) \sim \mathcal{D}_{in}^{train}} (\max(0, E(logits_{in}) - m_{in}))^2. \quad (9)$$

The first part is the cross-entropy part, where  $P(logits_{in})$  is the expected probability output, and  $f(\cdot)$  rep-

---

### Algorithm 1 Action-OOD Detection Algorithm

---

**Input:** Action skeleton data  $X$ ;

Graph structure  $G = \{g_{id}, g_{cf}, g_{cp}\}$ ;

Detection threshold  $\tau$  from training stage;

Algorithm running STAGE;

**Output:** Predict action label  $\hat{Y}$  for inference or value of loss function  $L$  in training stage.

```

1:  $F = f^{HD-GCN}(X, G)$  ▷ extract feature maps
2:  $\hat{F} = [F, ASH(F, p)]$  ▷ feature fusion block
3:  $F^{SE} = SELayer(\hat{F})$  ▷ detailed in Eqn. 6
4:  $F^{fuse} = MLP(F^{SE})$ 
5:  $logits = Classification(F^{fuse})$  ▷ detailed in Eqn. 8
6: if STAGE == ‘train’ then
7:   return  $L(logits)$  ▷ detailed in Eqn. 9
8: else
9:    $score = -E(logits)$  ▷ calculate energy score
10:  if  $score \geq \tau$  then
11:     $logits[-1] = 1$  ▷ detect as OOD
12:  end if
13:   $\hat{Y} = \text{argmax}(\text{softmax}(logits))$  ▷ get label through the normalized one-hot vector
14:  return  $\hat{Y}$ 
15:  Calculate evaluation metric.
16: end if

```

---

resents the model output on in-distribution training data. The second part is energy-based, where  $\mathcal{D}_{in}^{train}$  is the in-distribution training data,  $E(logits_{in})$  represents the energy score of in-distribution data,  $m_{in}$  is the margin parameter which is set before can help the ID energy score distribution reduce the variance and close to this point,  $\alpha$  is the tuning parameter that adjusts the proportion of energy part. With the help of this learning objective, the variance of ID data will be reduced. We can also ensure the model understand the energy score distribution of ID data, thus indirectly having the ability to distinguish ID and OOD samples. The overall process can be found in Algorithm 1.

## 4. Experiments

To demonstrate the human action detection accuracy of our proposed model Action-OOD, a series of experiments are conducted. In this section, we elucidate the intricate details of the experimental design and present

a thorough analysis of the experimental results. First, we introduce three datasets and describe their data pre-processing methods. Subsequently, we compare our work with other existing OOD detection methods and identify the proposed model’s strengths and weaknesses. Finally, we design three ablation studies to examine the effectiveness of individual modules.

#### 4.1. Dataset description

- **NTU-RGB+D 60 (Shahroudy et al., 2016) & 120 (Liu et al., 2019)**<sup>1</sup>: The NTU-RGB+D 60 dataset (NTU60) comprising 60 motion categories and 56,880 video samples, is extensively employed in diverse action recognition tasks. The NTU-RGB+D 120 dataset (NTU120) is an extension of the NTU-RGB+D 60 dataset, expanding the total number of human action categories to 120. Both datasets encompass 5 data modalities: 3D skeletons (body joints), masked depth maps, full-depth maps, RGB videos, and IR data. In this study, we exclusively utilize the 3D skeleton sequence data. The 3D skeleton data includes the 3D coordinates (X, Y, Z) of 25 body joints per frame and a maximum of 2 subjects. The actions in these datasets are categorized into three main groups: daily actions, interactive actions, and medical conditions. Five classes are randomly selected as unseen from the NTU60 dataset and ten classes from the NTU120 dataset. Note that these unseen categories encompass samples from all three categories.
- **Kinetics human action dataset (Kinetics 400)** (Kay et al., 2017): It is by far the largest unconstrained action recognition dataset constructed by DeepMind. It covers 400 action classes from human-object interactions to human-human interactions and some other complex interactions from YouTube videos. Since the Kinetics dataset provides only raw video clips without skeleton data, we adopt the skeleton-based action data processed by previous work STGCN (Yan et al., 2018)<sup>2</sup>. The processed data sequences contain 18 joints and 2 subjects. We randomly select

33 action classes marked as ‘unseen’ for OOD samples, ensuring the same ratio as used in NTU60 and NTU120.

- **Dataset splitting protocol:** Both our training set and validation set consist of data with known labels. Only the test set contains data from unknown categories. The seen class data in the validation set and the test set are consistent. The data volume ratio of the training set and test set/validation set in the known class data is 9:1. The number of samples in the train, validation, and test dataset is shown in Table 1.

Table 1: Number of samples in different data sets.

| Dataset     | Train   | Val    | Test (seen/unseen) |
|-------------|---------|--------|--------------------|
| NTU60       | 46,898  | 5,184  | 5,184/4,730        |
| NTU120      | 94,553  | 10,447 | 10,447/9,467       |
| Kinetics400 | 216,441 | 24,049 | 24,049/19,742      |

#### 4.2. Experiment details

##### 4.2.1. Experiment settings

- **Implementation details:** We adopt HD-GCN (Lee et al., 2023) as the backbone to extract Graph-structured skeleton data as shown in Fig. 1. The batch size of data is 64. The SGD optimizer is employed with a Nesterov momentum of 0.9 and a weight decay of 0.0004. The learning rate is 0.001 for NTU60 and NTU120 and 0.01 for Kinetics400. The number of learning epochs is set to 100 for NTU60 and NTU120, and 150 for Kinetics400, with a warm-up strategy (He et al., 2016) applied to the first five epochs for more stable learning. All our experiments are conducted on NVIDIA GeForce RTX 3090, CUDA 11.6 + PyTorch 1.12.1.
- **Evaluation metric:** As depicted in Fig. 4, we assess both the accuracy of detecting unseen samples and classifying seen samples. All samples under evaluation first undergo a threshold-based determination to discern whether their labels are unseen. If classified as ‘unseen’, they are marked accordingly; otherwise, they are predicted to belong to known categories. Regarding the unseen detection task, it can be viewed as a binary classification problem. We

<sup>1</sup><https://rose1.ntu.edu.sg/dataset/actionRecognition/>

<sup>2</sup><https://github.com/yysijie/st-gcn>



evaluate its accuracy using Detection Error (Liang et al., 2019), AUROC (Davis and Goadrich, 2006), and FPR at 95% TPR (Liang et al., 2019), following the methodology outlined in (Zhao et al., 2023). For action recognition tasks involving seen data, we employ Top-1 Accuracy (Lee et al., 2023) for quantitative evaluation. The details of these evaluation metrics are outlined as follows:

- 1) **Detection Error (Error)** (Liang et al., 2019): It measures the misclassification probability when the True Positive Rate (TPR) is 95%. The definition of an Error is:

$$Error = 0.5 \times (1 - TPR) + 0.5 \times FPR, \quad (10)$$

where *FPR* stands for False Positive Rate.

- 2) **AUROC** (Davis and Goadrich, 2006): It stands for the Area Under the Receiver Operating Characteristic (ROC) curve, which depicts the relation between TPR and FPR and ranges from 0 to 1 (the larger the value, the higher the accuracy). AUROC provides a single scalar value that summarizes the overall performance of a binary classifier across all possible thresholds.
- 3) **FPR at 95% TPR (FPR95)** (Liang et al., 2019): It refers to the rate of false positive predictions when the true positive rate reaches 95% in a classification task.
- 4) **Top-1 Accuracy (ACC)** (Lee et al., 2023): It measures the proportion of correctly predicted instances among all instances, where the predicted class label exactly matches the ground truth label for each instance. It is defined as:

$$ACC = \frac{hit}{N} \times 100\%, \quad (11)$$

where *hit* means the number of samples that were predicted correctly, and *N* represents the total number of test samples.

- 5) **Overlap**: For most energy-based OOD detection, the overlapping portion of the score distributions of ID and OOD indicates that OOD data is missed or ID data is misjudged as OOD. The smaller the overlap area of the two distributions, the greater the distinction between the

two data. Therefore, we propose to use the distribution overlap area for evaluation, which can more intuitively reflect the error of OOD recognition.

- **Loss function**: As introduced in section 3.3, we design a novelty energy loss to help the model distinguish OOD data during the training stage using only ID data. We set  $\alpha=0.1$  and  $m_{in}=-25$  in Eqn. 9.

#### 4.2.2. Baselines

Since most OOD detection models are post-hoc methods, we retain basic feature extraction parts and change different post-hoc methods to achieve OOD detection. We compare Action-OOD with four main methods: one score measuring method (**Maximum Softmax Probability, MSP** (Hendrycks and Gimpel, 2017)) and three different feature activation methods – **ReAct (Rectified Activation)** (Sun et al., 2021), **DICE (Directed Sparisification)** (Sun and Li, 2022), **DICE+ReAct**, **ASH (Activation Shaping)** (Djurisic and et al., 2023). Details are shown below:

- **MSP (Maximum Softmax Probability)**: (Hendrycks and Gimpel, 2017) claims that out-of-distribution examples tend to have lower maximum softmax probabilities than known samples. This scoring-based method has shown wide success in the computer vision area.
- **ReAct (Rectified Activation)** (Sun et al., 2021): A post-hoc method proposed to reduce the overconfidence problem of the model on OOD data by truncating activations on the penultimate layer of a network to limit the effect of noise.
- **DICE (Directed Sparisification)** (Sun and Li, 2022): Another post-hoc method, based on the idea of denoising useless information, sorts the weights of its contribution (i.e., weight  $\times$  activation). It claims that only a subset of units contributes to the in-distribution prediction results. However, it will result in non-negligible noise signals when measuring out-of-distribution data.
- **DICE + ReAct**: Following previous work (Djurisic and et al., 2023), we construct a baseline that filters out noise signals using both DICE and ReAct methods.

Table 2: Comparing the results of the OOD recognition task with other methods on the mixed OOD and ID test dataset. The best results are shown in bold.

| OOD          | NTU60        |              |              | NTU120       |              |              | Kinetics400  |              |              | Average      |              |              |
|--------------|--------------|--------------|--------------|--------------|--------------|--------------|--------------|--------------|--------------|--------------|--------------|--------------|
| Methods      | Error ↓      | FPR95 ↓      | AUROC ↑      | Error ↓      | FPR95 ↓      | AUROC ↑      | Error ↓      | FPR95 ↓      | AUROC ↑      | Error ↓      | FPR95 ↓      | AUROC ↑      |
| MSP          | 38.58        | 72.16        | 84.25        | 50.00        | 59.69        | 86.94        | <b>50.00</b> | 92.82        | 46.28        | 46.19        | 74.89        | 72.49        |
| ReAct        | 49.99        | 80.29        | 59.79        | 50.00        | 99.60        | 37.98        | 51.19        | 95.88        | 47.65        | 50.39        | 91.92        | 48.47        |
| DICE         | 52.47        | 99.95        | 35.62        | 24.24        | 56.40        | 84.84        | 51.12        | 96.16        | 46.34        | 42.61        | 84.17        | 55.60        |
| D+R          | 52.49        | 100.00       | 30.80        | 50.00        | 99.60        | 37.98        | 51.19        | 95.88        | 47.66        | 51.23        | 98.49        | 38.81        |
| ASH-P        | 26.87        | 58.33        | 84.48        | 21.12        | 56.78        | 86.20        | 50.16        | 92.55        | 46.75        | 32.72        | 69.22        | 72.48        |
| ASH-S        | 50.00        | 59.77        | 78.73        | 50.00        | 60.72        | 85.46        | 51.22        | 95.74        | 48.82        | 50.41        | 72.08        | 71.00        |
| ASH-B        | 42.72        | 78.77        | 68.43        | 49.99        | 58.53        | 85.96        | 51.11        | 96.25        | 46.72        | 47.94        | 77.85        | 67.04        |
| <b>ours</b>  |              |              |              |              |              |              |              |              |              |              |              |              |
| <b>ASH-P</b> | 30.42        | <b>52.68</b> | <b>86.64</b> | 21.36        | 60.64        | 86.40        | 51.37        | <b>90.61</b> | <b>50.43</b> | 34.38        | <b>67.98</b> | <b>74.49</b> |
| <b>ours</b>  |              |              |              |              |              |              |              |              |              |              |              |              |
| <b>ASH-S</b> | 33.72        | 62.45        | 84.10        | 37.87        | 59.67        | 85.09        | 50.37        | 93.67        | 48.23        | 40.65        | 71.93        | 72.47        |
| <b>ours</b>  |              |              |              |              |              |              |              |              |              |              |              |              |
| <b>ASH-B</b> | <b>30.21</b> | 55.43        | 85.98        | <b>19.57</b> | <b>56.11</b> | <b>87.17</b> | 51.25        | 95.62        | 47.17        | <b>33.68</b> | 69.05        | 73.44        |

- **ASH (Activation Shaping)** (Djurisic and et al., 2023): It consists of three different mechanisms to conduct pruning-based feature activation shaping, including ASH-P, ASH-S, and ASH-B.

#### 4.2.3. Ablation study

To verify the effectiveness, we design ablation studies on the following components of Action-OOD.

- **GCN**: This is designed to measure the effect of the feature fusion block of Action-OOD. As previously mentioned, Action-OOD has two parts of features: GCN-based features, which excel in classifying in-distribution (ID) samples, and ASH-based features, which aim to reduce overconfidence in predictions for OOD samples. This experiment can prove the improvement effect of ASH operation on the model OOD recognition task.
- **ASH**: Based on the analysis of previous work, a pruning strategy that solely relies on thresholding may prove inadequate in certain scenarios, thus affecting the OOD recognition effect of the model. To verify whether such a problem also exists in unseen action detection, and to illustrate the role of the feature fusion module, we design such an ablation study experiment.
- **CE Loss**: To demonstrate the effect of the proposed energy loss function, we conduct experiments by training with conventional CE loss only.

### 4.3. Results and discussion

#### 4.3.1. Performance comparison against baselines

We evaluate the proposed Action-OOD method against baselines across three datasets for two tasks: (a) to distinguish OOD samples from an ID and OOD mixture dataset, and (b) to evaluate whether ID samples will be misclassified as OOD merely based on ID data. We also provide the average results for all models involved across the three datasets.

As seen from Table 2, our method achieves the best performance in most metrics on the ID-OOD mixed test dataset. On the NTU60 dataset, our method achieves an average AUROC of 85.57% for OOD detection, with the accuracy of seen classification exceeding 91% in Table 3. Compared with several post-hoc methods, the average AUROC increases by 43.48%. Based on the average three evaluation metrics on the three data sets, our method also achieves the best results. To some extent, our method alleviates the problem of overconfidence in the trained model when facing OOD samples using only an end-to-end model.

For the ID sample-only evaluation in Table 3, the best accuracy in ID multi-class classification may sometimes be achieved by other methods, especially in the NTU60 dataset. However, these methods show poor performance in OOD detection tasks (see Table 2), which means that the model still recognizes most of the data as ID. Consequently, the issue of overconfidence persists. Nevertheless, based on the average performance of the three data sets, our method still obtains the highest classification accuracy in the ID sample-only test. In summary,

Table 3: Comparing the results of the ID multi-class classification task with other methods on the ID sample-only test dataset. The best results are shown in bold.

| ID<br>Methods     | NTU60           |                      | NTU120          |                      | Kinetics400     |                      | Average         |                      |
|-------------------|-----------------|----------------------|-----------------|----------------------|-----------------|----------------------|-----------------|----------------------|
|                   | Top1 $\uparrow$ | Overlap $\downarrow$ | Top1 $\uparrow$ | Overlap $\downarrow$ | Top1 $\uparrow$ | Overlap $\downarrow$ | Top1 $\uparrow$ | Overlap $\downarrow$ |
| MSP               | 91.69           | <b>0.35</b>          | 89.64           | 0.41                 | 22.39           | <b>0.88</b>          | 67.91           | <b>0.55</b>          |
| ReAct             | 88.27           | 0.83                 | 83.82           | 0.80                 | 20.98           | 0.95                 | 64.36           | 0.86                 |
| DICE              | <b>94.23</b>    | 0.72                 | 76.29           | 0.47                 | 21.37           | 0.93                 | 63.96           | 0.71                 |
| D+R               | 92.76           | 0.67                 | 47.54           | 0.78                 | 20.37           | 0.95                 | 53.56           | 0.80                 |
| ASH-P             | 91.32           | 0.45                 | 88.91           | 0.43                 | 25.18           | 0.92                 | 68.47           | 0.60                 |
| ASH-S             | 91.39           | 0.55                 | 89.35           | 0.45                 | 23.84           | 0.98                 | 68.19           | 0.66                 |
| ASH-B             | 89.69           | 0.73                 | 88.98           | 0.42                 | 20.81           | 0.94                 | 66.49           | 0.70                 |
| <b>ours-ASH-P</b> | 91.94           | 0.39                 | <b>89.84</b>    | 0.40                 | <b>26.18</b>    | 0.89                 | <b>69.32</b>    | 0.56                 |
| <b>ours-ASH-S</b> | 91.22           | 0.42                 | 88.98           | 0.43                 | 23.22           | 0.90                 | 67.81           | 0.58                 |
| <b>ours-ASH-B</b> | 91.61           | 0.41                 | 89.13           | <b>0.39</b>          | 25.04           | 0.95                 | 68.59           | 0.58                 |

our method maintains the accuracy of ID data classification while also ensuring effective detection capability for OOD tasks.

It can be observed that compared to the first two datasets, the overall prediction accuracy on Kinetics is not satisfactory. Additionally, the direct classification results on the ID dataset are relatively poor. By comparing the incorrectly predicted samples on the Kinetics data set, we discover that some ID samples are misclassified as OOD samples, which means that the model lacks confidence in the ID samples. This also shows to some extent that the data itself may lack expressive power, which prevents the model itself from learning more distinguishing features. One possible reason could be attributed to the graph construction as shown in Fig. 2. Firstly, the Kinetics dataset itself includes a large number of actions involving interactions between people and objects, making it difficult to distinguish using skeleton data only. Secondly, through our visualization analysis, there are certain issues in extracting Kinetics nodes in the STGCN (Yan et al., 2018). For instance, nodes 15 and 16 in the data represent the left and right eyes respectively. However, these nodes may not provide much information about the actions. Moreover, while the dataset models the left and right hips separately, it lacks crucial information about the key body waist nodes, which are essential for understanding the type of limb movement.

#### 4.3.2. Number of dimensions for OOD representation

Using machine learning methods to process categorical data generally requires one-hot encoding of category labels in the data. The processed vectors are then input into

the model to participate in training. The dimension of the encoding vector is generally equal to the total number of data categories. In our work, to make the model realize that there are other unknown categories besides the ID category, an additional  $k$ -dimensional vector is concatenated to mark whether the data belongs to OOD. The experimental results on the NTU60 dataset are shown in Table 4.

The last two rows indicate the results that we use additional dimensions ( $k = 1$  and  $k = 3$ ) in the embedding to represent OOD samples. Since the training set consists only of ID samples, there are no samples with these extra dimensions set to 1. We hope this operation can effectively inform the model during training that all samples belong to the first 55 classes and not to the 56th class or the 56th-58th classes, providing it with extra information. By comparing the results in the table for the rows "55", "58 (55+3)", and "56 (55+1)", it can be observed that using the additional dimension indeed improves the model's accuracy of OOD detection. This further validates the effectiveness of our design.

Table 4: Ablation experiment results reflect the performance of each module. The bold numbers represent the best performance.

| NTU60     | Unseen             |                    |                  | Seen            |                      |
|-----------|--------------------|--------------------|------------------|-----------------|----------------------|
|           | Error $\downarrow$ | FPR95 $\downarrow$ | AUROC $\uparrow$ | Top1 $\uparrow$ | Overlap $\downarrow$ |
| 55        | 34.58              | 64.16              | 83.57            | 91.59           | 0.41                 |
| 58 (55+3) | 33.49              | 61.99              | 85.66            | 91.49           | 0.41                 |
| 56 (55+1) | <b>30.42</b>       | <b>52.68</b>       | <b>86.64</b>     | <b>91.94</b>    | <b>0.39</b>          |

At the same time, comparing the results using 56(55+1) and 58(55+3) dimensions, reveals that using an extra 1 dim is more effective than that of 3 dims. Perhaps it

is because higher-dimensional representations can easily cause information redundancy, which makes training difficult. Therefore, the experimental results in this paper all use additional 1-dimensional vectors to represent the OOD classes. It should be noted that perhaps it would be better to use more dimensional representations for the NTU120 and Kinetics400 datasets, but the 1-dimensional OOD representation method is used here for the requirement of comparison.

#### 4.3.3. Ablation study

**Effect of Activation Shaping:** Comparing the results of the GCN with ours, it shows that with the help of the ASH strategy, the Error metric decreases by 58.59%. AUROC accuracy also improves by 79.12%. ASH can significantly improve the OOD recognition ability of the model. At the same time, it can be seen from the table that the seen accuracy in the GCN experiment is very low because the energy score distribution of unseen and seen has a high degree of overlap. Therefore, many ID samples will be misidentified as OOD. The OOD detection method that uses the energy score of the ranked 10% ID sample as the threshold in OOD detection is suspected of overcorrecting the performance of this model.

Table 5: Ablation experiment results reflect the performance of each module. The bold numbers represent the best performance.

| NTU60   | OOD          |              |              | ID           |             |
|---------|--------------|--------------|--------------|--------------|-------------|
|         | Error ↓      | FPR95 ↓      | AUROC ↑      | Top1 ↑       | Overlap ↓   |
| GCN     | 49.31        | 93.61        | 48.37        | 7.24         | 0.89        |
| ASH     | 34.33        | 63.66        | 78.22        | 90.66        | 0.59        |
| CE Loss | 37.51        | 70.02        | 79.58        | 91.61        | 0.49        |
| ours    | <b>30.42</b> | <b>52.68</b> | <b>86.64</b> | <b>91.94</b> | <b>0.39</b> |

**Effect of Feature Fusion Block:** Comparing it to the column ASH, leveraging typical GCN embeddings results in an 11.39% increase in the Error metric and an 8.42 percentage increase in AUROC accuracy. When considering the experimental outcomes from the GCN scenario, it becomes evident that the feature fusion module empowers the model to increase the accuracy of out-of-distribution (OOD) detection without compromising its ability to recognize in-distribution (ID) samples.

**Effect of Energy Loss:** Comparing the results with only traditional cross-entropy loss (bottom two rows), it can be observed that the method utilizing energy loss employed in this paper significantly enhances the model’s

capabilities across various settings. Additionally, we discover that compared with directly employing ASH, the model trained with the feature fusion module but using only cross-entropy loss performs less effectively on OOD tasks, yet slightly outperforms in ID classification. This further indicates that the combined usage of the feature fusion module and energy loss can address the overall capabilities of the model, leading to better differentiation between in-distribution and out-of-distribution data.

#### 4.3.4. Different pruning percentages

To explore the effect of pruning percentage  $p$ , different values are tested in our experiments. As shown in Fig. 5, we select the best-performing ASH-P strategy on the NTU60 data set for evaluation. The size of the blue points reflects the size of the pruning ratio  $p$ . The red, green, and purple points respectively represent the performance of the ReAct, DICE, and DICE+ReAct methods at their optimal ratios.

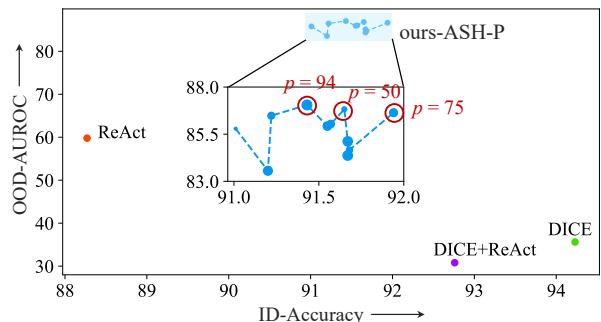


Figure 5: ID-OOD tradeoff on NTU-RGB+D 60 dataset. The size of the points in the enlarged line chart corresponds to different  $p$  values. The line chart represents the results of our method taking  $p$ -values in the range of 40%-90%.

The data points located closer to the upper-right corner of the figure exhibit superior performance. Our approach achieves optimal results when integrated with the ASH strategy. Concerning the OOD detection task across various  $p$  values, it is apparent that the correlation between accuracy and  $p$  value is nonlinear. To balance the accuracy between OOD and ID samples, we choose the  $p$ -value of 75 as the best pruning percentage.

## 5. Conclusion and future works

This paper introduces Action-OOD, an end-to-end framework designed to address the challenge of recognizing out-of-distribution human action samples. The framework adopts a hierarchical graph composition method and utilizes GCN for extracting the feature maps of human skeletons. Subsequently, a feature activation strategy is applied and we fuse the activated features with the original ones through a proposed feature fusion block. Experiments show that this step helps to equip the model with the innate ability to identify out-of-distribution data while still maintaining the capability of ID classification. Next, an energy score value is computed for each test sample based on the logits output by the classifier. This helps determine whether it belongs to an OOD category. The model is trained using a designed energy-based loss function, which helps the model to reduce the variance of ID data and differentiate ID and OOD samples. Experimental results demonstrate that this approach effectively mitigates the overconfidence issue encountered by human action classification models when dealing with samples beyond the training category. Notably, since the model training process relies exclusively on sample information within the branch without prior knowledge of OOD distribution characteristics, it exhibits broad practical applicability.

Admittedly, the model still needs to address some potential limitations. Firstly, since the model is trained on GCN, its generalization ability is constrained by the number of skeleton nodes across various datasets. In real-world scenarios, if the trained model is deployed to identify whether a test sample with a different number of nodes is out-of-distribution, its accuracy may be compromised. Secondly, the end-to-end model’s generalization capability is still bounded by the model parameters and the size of the dataset. One potential solution is to explore semi-supervised learning techniques to mitigate this issue. Moreover, the problem can be further addressed by integrating a large language model and conducting training on datasets with limited ID samples. By leveraging existing category text and feature information, the model can infer the name of the unknown category for unfamiliar sample features. In summary, human action recognition tasks present diverse application scenarios, with numerous novel challenges awaiting exploration based on

specific practical contexts.

## References

- Chen, Y., Zhang, Z., Yuan, C., Li, B., Deng, Y., Hu, W., 2021. Channel-wise topology refinement graph convolution for skeleton-based action recognition, in: Proceedings of the IEEE/CVF international conference on computer vision, pp. 13359–13368.
- Cheng, K., Zhang, Y., Cao, C., Shi, L., Cheng, J., Lu, H., 2020. Decoupling gcn with dropgraph module for skeleton-based action recognition, in: Computer Vision–ECCV 2020: 16th European Conference, Glasgow, UK, August 23–28, 2020, Proceedings, Part XXIV 16, Springer. pp. 536–553.
- Chéron, G., Laptev, I., Schmid, C., 2015. P-cnn: Pose-based cnn features for action recognition, in: Proceedings of the IEEE international conference on computer vision, pp. 3218–3226.
- Davis, J., Goadrich, M., 2006. The relationship between precision-recall and roc curves, in: Proceedings of the 23rd international conference on Machine learning, pp. 233–240.
- Djurisic, A., et al., 2023. Extremely simple activation shaping for out-of-distribution detection .
- Geiger, A., Lenz, P., Urtasun, R., 2012. Are we ready for autonomous driving? the kitti vision benchmark suite, in: 2012 IEEE conference on computer vision and pattern recognition, IEEE. pp. 3354–3361.
- He, K., Zhang, X., Ren, S., Sun, J., 2016. Deep residual learning for image recognition, in: Proceedings of the IEEE conference on computer vision and pattern recognition, pp. 770–778.
- Hein, M., Andriushchenko, M., Bitterwolf, J., 2019. Why relu networks yield high-confidence predictions far away from the training data and how to mitigate the problem, in: Proceedings of the IEEE/CVF conference on computer vision and pattern recognition, pp. 41–50.
- Hendrycks, D., Basart, S., Mazeika, M., Zou, A., Kwon, J., Mostajabi, M., Steinhardt, J., Song, D., 2022. Scaling out-of-distribution detection for real-world settings. International Conference on Machine Learning .

- Hendrycks, D., Gimpel, K., 2017. A baseline for detecting misclassified and out-of-distribution examples in neural networks. *Proceedings of International Conference on Learning Representations* .
- Hu, J., Shen, L., Sun, G., 2018. Squeeze-and-excitation networks, in: *Proceedings of the IEEE conference on computer vision and pattern recognition*, pp. 7132–7141.
- Jiang, Y.G., Dai, Q., Liu, W., Xue, X., Ngo, C.W., 2015. Human action recognition in unconstrained videos by explicit motion modeling. *IEEE Transactions on Image Processing* 24, 3781–3795.
- Kay, W., Carreira, J., Simonyan, K., Zhang, B., Hillier, C., Vijayanarasimhan, S., Viola, F., Green, T., Back, T., Natsev, P., et al., 2017. The kinetics human action video dataset. *arXiv preprint arXiv:1705.06950* .
- Kipf, T.N., Welling, M., 2017. Semi-supervised classification with graph convolutional networks, in: *International Conference on Learning Representations (ICLR)*.
- LeCun, Y., Chopra, S., Hadsell, R., Ranzato, M., Huang, F., 2006. A tutorial on energy-based learning. *Predicting structured data 1*.
- Lee, J., Lee, M., Lee, D., Lee, S., 2023. Hierarchically decomposed graph convolutional networks for skeleton-based action recognition, in: *Proceedings of the IEEE/CVF International Conference on Computer Vision*, pp. 10444–10453.
- Liang, S., Li, Y., Srikant, R., 2019. Enhancing the reliability of out-of-distribution image detection in neural networks .
- Liu, J., Shahroudy, A., Perez, M., Wang, G., Duan, L.Y., Kot, A.C., 2019. Ntu rgb+ d 120: A large-scale benchmark for 3d human activity understanding. *IEEE transactions on pattern analysis and machine intelligence* 42, 2684–2701.
- Liu, J., Wang, G., Hu, P., Duan, L.Y., Kot, A.C., 2017a. Global context-aware attention lstm networks for 3d action recognition, in: *Proceedings of the IEEE conference on computer vision and pattern recognition*, pp. 1647–1656.
- Liu, M., Liu, H., Chen, C., 2017b. Enhanced skeleton visualization for view invariant human action recognition. *Pattern Recognition* 68, 346–362.
- Liu, X., Lochman, Y., Zach, C., 2023. Gen: Pushing the limits of softmax-based out-of-distribution detection, in: *Proceedings of the IEEE/CVF Conference on Computer Vision and Pattern Recognition*, pp. 23946–23955.
- Nalisnick, E., Matsukawa, A., Teh, Y.W., Gorur, D., Lakshminarayanan, B., 2019. Do deep generative models know what they don’t know? .
- Nguyen, A., Yosinski, J., Clune, J., 2015. Deep neural networks are easily fooled: High confidence predictions for unrecognizable images, in: *Proceedings of the IEEE conference on computer vision and pattern recognition*, pp. 427–436.
- Nikam, A.S., Ambekar, A.G., 2016. Sign language recognition using image based hand gesture recognition techniques, in: *2016 Online International Conference on Green Engineering and Technologies (IC-GET)*.
- Schlegl, T., Seeböck, P., Waldstein, S.M., Schmidt-Erfurth, U., Langs, G., 2017. Unsupervised anomaly detection with generative adversarial networks to guide marker discovery, in: *International conference on information processing in medical imaging*, Springer. pp. 146–157.
- Shahroudy, A., Liu, J., Ng, T.T., Wang, G., 2016. Ntu rgb+ d: A large scale dataset for 3d human activity analysis, in: *Proceedings of the IEEE conference on computer vision and pattern recognition*, pp. 1010–1019.
- Simonyan, K., Zisserman, A., 2014. Two-stream convolutional networks for action recognition in videos. *Advances in neural information processing systems* 27.
- Song, Y., Sebe, N., Wang, W., 2022. Rankfeat: Rank-1 feature removal for out-of-distribution detection. *Advances in Neural Information Processing Systems* 35, 17885–17898.
- Sun, Y., Guo, C., Li, Y., 2021. React: Out-of-distribution detection with rectified activations, in: *Advances in Neural Information Processing Systems*.

- Sun, Y., Li, Y., 2022. Dice: Leveraging sparsification for out-of-distribution detection, in: European Conference on Computer Vision.
- Wang, H., Wang, L., 2017. Modeling temporal dynamics and spatial configurations of actions using two-stream recurrent neural networks, in: Proceedings of the IEEE conference on computer vision and pattern recognition, pp. 499–508.
- Wu, Q., et al., 2023. Energy-based out-of-distribution detection for graph neural networks, in: International Conference on Learning Representations (ICLR).
- Yan, S., Xiong, Y., Lin, D., 2018. Spatial temporal graph convolutional networks for skeleton-based action recognition, in: Proceedings of the AAAI conference on artificial intelligence.
- Yu, W., et al., 2022. Metaformer is actually what you need for vision, in: IEEE Conference on Computer Vision and Pattern Recognition, pp. 10819–10829.
- Yu, Y., Shin, S., Ko, M., Lee, K., 2024. Exploring using jigsaw puzzles for out-of-distribution detection. Computer Vision and Image Understanding , 103968.
- Zhang, J., et al., 2023. Openood v1. 5: Enhanced benchmark for out-of-distribution detection. arXiv preprint arXiv:2306.09301 .
- Zhao, C., Du, D., Hoogs, A., Funk, C., 2023. Open set action recognition via multi-label evidential learning, in: Proceedings of the IEEE/CVF Conference on Computer Vision and Pattern Recognition, pp. 22982–22991.
- Zhu, Y., Chen, Y., Xie, C., Li, X., Zhang, R., Xue, H., Tian, X., Chen, Y., et al., 2022. Boosting out-of-distribution detection with typical features. Advances in Neural Information Processing Systems 35, 20758–20769.